First-principles study of electronic properties of hydrogenated graphite

A. Allouche* and Y. Ferro
Physique des Interactions Ioniques et Moléculaires, Université de Provence and CNRS (UMR 6633), Campus Universitaire de Saint Jérôme, Case 242, 13397 Marseille Cedex 20, France
(Received 13 July 2006; revised manuscript received 26 September 2006; published 15 December 2006)

Progressive implantation of hydrogen atoms into graphite is modeled by first-principles density functional theory. The maximum H/C ratio was found at 53%, which is in good agreement with experimental results. The hydrogen trapping energy varies from −0.7 eV at very low concentrations to a limit of −1.9 eV at saturation. Special attention is given to the electronic density of states at each step of the process; they are compared to the experimental spectra from electron spectroscopy on graphite hydrogenated by energetic ions bombardment. The density of states of the fully hydrogenated graphite is compared to that of diamond. Step-by-step study of the π^* density of states starting from pure graphite (all sp^2 carbon) leads to a criterion of characterization of graphitic materials amorphization. The calculated sp^3/sp^2 ratio in hydrogenated graphite is proposed as a model to quantify the rate of tetrahedral carbon atoms in amorphous and hydrogenated amorphous carbon samples.

DOI: 10.1103/PhysRevB.74.235426 PACS number(s): 73.43.Cd, 73.20.At, 79.20.Uv

I. INTRODUCTION

Carbon and carbon-based materials have been extensively studied for plasma facing components (PFC) in magnetic confinement fusion reactors (tokamaks).[1–5] In this application, hydrogen retention is an impediment whereas the great propensity of these materials to store hydrogen is actively sought after in other areas.[6–8] This property is mainly due to the unique ability of carbon atoms to organize into plane trigonal structures, such as in graphite where they adopt the sp^2 hybridization pattern, or to easily evolve towards tetrahedral structures typical of sp^3 hybridization like in diamond.

More or less perfect graphite has proven to be a good model for quantum study of hydrogen interaction with carbonaceous materials in these areas of interest. Attention was given to atomic hydrogen adsorption on bare (0001) graphite surfaces,[9] on zigzag edges,[10] or on atomic vacancies on the basal plane.[11] In these contributions, the quantum results were validated through comparison with temperature-programmed desorption spectroscopy (TPD), or with vibrational spectroscopy, mainly high-resolution electron energy loss spectroscopy (HREELS).[12] These techniques are typical of surface physics and are not applicable when the bulk of the solid is concerned. Hydrogen implantation and carbon hybridization characterization are more often studied using the tools of electron spectroscopy techniques such as electron energy-loss spectroscopy (EELS)[13] or X-ray absorption spectroscopy (XPS, Auger spectroscopy, C K VV…).[14–17] The signal recorded by these techniques is directly related to the electronic density of states (DOS) of the material under study. Therefore, this paper is more specifically focused on the quantum evaluation of the DOS. Special attention will given to the relative positions of the $\sigma-\sigma^*$ and $\pi-\pi^*$ bands because of their crucial role in these spectroscopies and because it is important to obtain any possible information on the evolution of the spectra with a view to quantifying hydrogen retention into graphitic materials. In the special domain of tokamak physics, the problem of hydrogen isotopes retention into graphitic PFC is of uppermost importance. This retention can primarily be quantified by post-mortem analysis of samples exposed to hydrogen plasma action. Laboratory simulations are performed by ion beam bombardment. In both cases, the analysis is carried out using the above-mentioned spectroscopies. The hydrogen retention transforms some carbon atom structures from sp^2 to sp^3 and this is reflected in the DOS. Therefore, comparison of electronic spectra and quantum DOS is the best approach to evaluate the hydrogen retention[18] and references therein.

Since H retention induces a certain amorphization of the material, the former domain can be naturally related to another question that has attracted much research concerning the structure of amorphous carbons, i.e., pure (*a*-C) or hydrogenated (*a*-C:H). Amorphous carbon is a very attractive material since it can be almost as hard as diamond.[19] It is also chemically inert and features interesting properties for semiconductor applications. Amorphous carbon *a*-C, as well as *a*-C:H, characterization is very often performed through sp^3/sp^2 ratio estimation. Theoretically, the atomic structure of these materials is difficult to model due to the wide variety of configurations carbon atoms can support.[20] Therefore, although amorphous carbon is not the first objective of this paper, from the quantum modeling viewpoint this focus is compatible with the first one insofar as electronic structure and hybridization modes are concerned and the bulk-hydrogenated graphite can be a useful reference since its structure is simpler and well defined.

Based on the above considerations, the present paper is organized as follows. Section II gives an overview of the computation methods and also proposes a discussion on pure graphite DOS. The main features are described and compared to experimental DOS. This section is presented as a validation of the method.

In Sec. III, the graphite crystal cell is gradually saturated with hydrogen atoms trapped into the bulk. The most characteristic steps of this process are described together with the associated DOS which evolves from a structure similar to graphite to an increasingly perturbed structure.

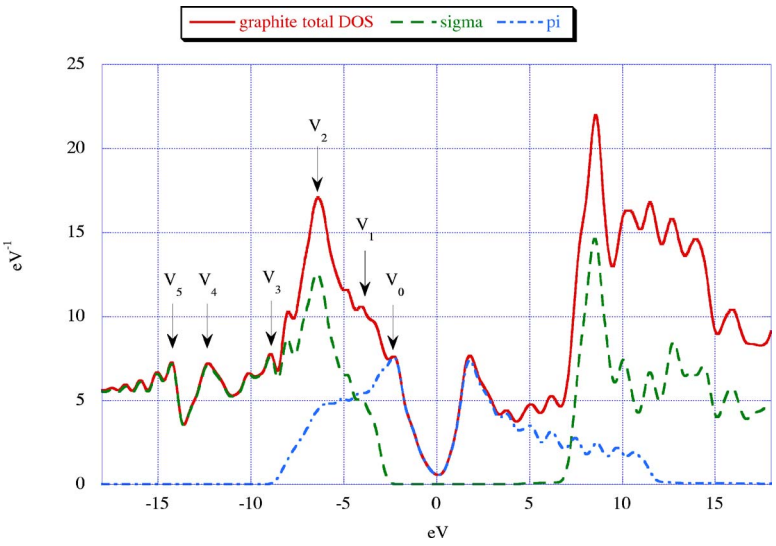

FIG. 1. (Color online) Pure graphite DOS (eV), the Fermi energy level is taken as the origin of energy. The V_0 to V_5 peaks are assigned according to Lascovich *et al.* (Ref. 14). Definition of the σ and π projection is given in the text. In this figure, and also in Figs. 4–6, the DOS zero is set to the Fermi energy of the systems.

In the discussion, the results gathered in Sec. III are analyzed and compared to experimental results derived from hydrogen bombardment of the graphite surface or amorphous carbon and hydrogenated amorphous carbons.

II. COMPUTATIONAL SECTION AND ELECTRONIC STRUCTURE OF THE GRAPHITE SUBSTRATE

The calculations were performed within the framework of the spin-polarized gradient-corrected density functional theory (DFT). The exchange, as well as the correlation, functionals are Perdew-Burke-Ernzerhof (PBE).[21] A plane-wave basis set was used with an energy cutoff of 32 Rydberg (435 eV); the ionic core potential was modeled using the Vanderbilt ultrasoft pseudopotentials.[22] Integration in the first Brillouin zone was performed using the $6\times6\times6$ points Monkhorst-Pack[23] sampling.

The dimensions of the primitive hexagonal unit cell were optimized while keeping unchanged the experimental ratio $\mathbf{c}/\mathbf{a}=2.72$. This yielded the following cell parameters $\mathbf{a}=2.466$ Å, $\mathbf{c}=6.721$ Å, which corresponds to a C-C bond length of 1.424 Å. Hydrogen trapping in the interlayer space was modeled using the $3\times3\times1$ supercell with parameter $\mathbf{a}=7.398$ Å, containing 36 carbon atoms distributed across two layers. Considering that first-principles DFT yields very poor results in the case of weak or van der Waals interactions and considering that the interplane cohesion in graphite is insured by this kind of forces, it seems very unreliable to optimize the cell parameters (specially the **c** one) along the hydrogen trapping modeling. Therefore, the cell parameters were kept unchanged during the whole calculation.

Also, the case of molecular hydrogen trapping is not considered because a preliminary calculation within the same framework showed that the trapping of even a single H_2 molecule is highly unstable [total reaction energy $E(H_2 \text{ in bulk})-E(H_2)-E(\text{bulk})=+3.7$ eV].

The stationary state structures of hydrogen inclusion were determined by placing H above any candidate adsorbent C and optimizing the geometry using the quasi-Newton Broyden-Fletcher-Goldfarb-Shanno generalized algorithm. All the atoms were included in the optimization procedure, without any geometrical limitation. All the energy calculations were made using the *Quantum-Espresso* package.[24]

The procedure for step-by-step optimization of the hydrogenated systems has been described in a previous publication.[9] During this process the crystal parameters are kept unchanged. The hydrogen–graphite bulk binding energy was calculated using two definitions:

(i) The successive energies were calculated using Eq. (1)

$$\Delta E^n = (E^n - E^{n-1} - E^H), \tag{1}$$

where E^n is the total energy of the system after incorporation of n hydrogen atoms, E^H is the isolated hydrogen atom energy.

(ii) The average binding energy is calculated using the following equation:

$$\Delta E_A^n = (E^n - nE^H)/n. \tag{2}$$

The density of states (DOS) was calculated using a smoothing of 0.03 Rydberg (0.4 eV); a similar smoothing (0.5 eV) had been applied in Ref. 25. In the high-energy domain within the conduction band, the DOS is especially dependent on the total number of electronic bands calculated for each k point. Moreover, since the goal is to compare the DOS of various physical systems, the number of electronic bands was set to 200 for all DOS calculations and all systems, whether pure or hydrogenated. In all cases, this number of bands is large enough to describe the DOS up to a cutoff value of 20 eV above the Fermi level. For the pure graphite working cell, this number of bands fairly accurately reproduces the DOS calculated on the primitive crystal unit cell using a much larger number of k point ($36\times36\times36$). The DOS zero is always placed at the Fermi energy of each considered system.

The pure graphite DOS is displayed in Fig. 1. In this section and the following, we denoted as σ contribution the sum of the projections on $2s$, $2p_x$, and $2p_y$ carbon orbitals, and π indicates the projection on the C($2p_z$). This convention is also applied to the hydrogenated systems. This rather rough definition is imposed by the plane-wave expansion of

TABLE I. Main features of the pure graphite DOS (in eV) compared to electronic spectroscopy and to other theoretical results. The peak designation (also shown in Fig. 1) and the numerical values are taken from Lascovich *et al.* (Ref. 14).

	V_0	V_1	V_2	V_3	V_4	V_5
Ugolini *et al.* (Ref. 13) UPS	2.8	4.8	8.2		12.8	
Lascovich *et al.* (Ref. 14) XPS	~2.5	4	~7–8			
Lascovich *et al.* (Ref. 14) XAES	0.9/2	4.4	7.6	8.9	13.2	14.7
Willis *et al.* (Ref. 32) Theory: High energy band-structure calculation	2.3	4.5	7.8	9.2	12.5	15.4
Charlier*et al.* (Ref. 24) Theory: First-principles DFT (Ref. 24)	2.3	3.6	6.9	9	13.1	15.1
Experimental mean values given in Ref. 14	2.8	4.7	8.0		13.6	15.6
Theoretical mean values given in Ref. 14	2.3	4.2	7.0	8.8	12.4	14.9
This work	2.3	3.9	6.4	8.9	12.3	14.2

the crystal orbitals which makes it very difficult to build localized hybrid orbitals.

In the valence band, the pure σ band extends from −20 to −9 eV, the Fermi level being taken as the reference of energy. The peaks below −14 eV correspond to almost pure C(2*s*) components.

The pure π band overlaps with the σ band from −9 to −2.4 eV. The larger σ peak is at −6.4 eV and the π peak at −2.3 eV. In the conduction band, the main π^* peak is at 1.9 eV and the σ^* one at 8.6 eV. The π^* peaks extend up to 12 eV and overlap with the σ^* band from 7 to 12 eV.

These features are in good agreement with experimental and theoretical results exposed by Titantah *et al.*[16] The C K ELNES energy difference between the main π^* and σ^* peaks is −6.4 eV, the HEELS experimental value is $6<7$ eV and as per the present results is 6.8 eV. The carbon *K* near-edge X-ray-absorption spectra[26] also yield a distance of 7 eV.

In Table I, a comparison is made with electron spectroscopy and other theoretical works mentioned in Lascovich *et al.*[14] The features data given by these authors are tentatively assigned in Fig. 1. The general agreement is very good with both series of data, experimental and theoretical mean values, collected in Table I. The only noticeable discrepancy concerns the V_2 signal, which is undervalued by 0.6 eV versus the calculated mean value.

The parts of the DOSs that cannot be projected on C(2*s*) or C(2*p*) should be projected on higher angular momentum localized orbitals. Therefore, these electronic states are associated to polarization and diffuse contributions, they are generally ascribed to the interlayer electron density. This is the case in the 4.3 to 7 eV zone, the major contribution included in the surface delimited by the total DOS and the π projection is neither π^* nor σ^*. Fisher *et al.*[26] assigned to the interlayer states those peaks situated approximately 4 eV above the π^* peak in the C K NEXAFS spectra of polycrystalline graphite and they likened these peaks to those in the same domain of the theoretical DOS they had taken as a reference. Therefore, the two structures at 3.3 and 4.5 eV in Fig. 1 can be ascribed to interlayer states.

III. HYDROGEN ATOMS INSERTION IN THE INTERLAYER REGION

The successive absorption energies displayed in Fig. 2 are similar to the adsorption energy pattern previously published on graphite step edges.[10] The first hydrogen that is inserted breaks the delocalized π electrons system. The bare graphite plane is not very reactive and the binding energy is low, i.e., −0.68 eV, similar to the adsorption energy on the bare graphite surface.[27–30] But the next three implanted hydrogens take advantage of the induced perturbation of the graphene electronic structure and their interaction energies are larger. In this process, the odd-numbered H atoms interact with a closed shell system and leave a radical-type configuration with an unpaired π electron, therefore a more reactive configuration. This explains the serrated aspect of the successive absorption energies in Fig. 2 and already discussed in Ref. 10. For all the situations described in this work, the total spin polarization of these systems is 0 when the number of hydrogens is even, and 1.0 dispersed across several carbon atoms when the number of hydrogens is odd.

The same tendency to adsorb in cluster pattern reported in Ref. 12 is again noted here: the first six atoms are bonded to the same hexagonal cycle, but now equally distributed across the two sides of the original plane, eventually forming a boat-shaped structure after binding of the first six hydrogens. Special attention must be given to hydrogens numbers 5 and 6. H#5 interacts with the last double bond of the cycle, so its individual interaction energy is lower than the preceding ones, but H#6 meets the last unpaired electron, hence the corresponding energy is quite high.

Hydrogen #7 is absorbed on the upper side of the other graphene plane. Since it interacts with a bare surface, the binding energy is again very low, −0.83 eV, but larger than for H#1. This can be explained by the upper layer geometry which is slightly perturbed by the adsorption of the first 6 Hs, therefore the layer is no more exactly plane and the carbon atoms are not strictly sp^2.

With H#8, the average binding energy reaches a limit around −1.8 eV, it is bonded also on the upper plane, besides H#7 and in *trans* position, H#9 forms a triplet structure with

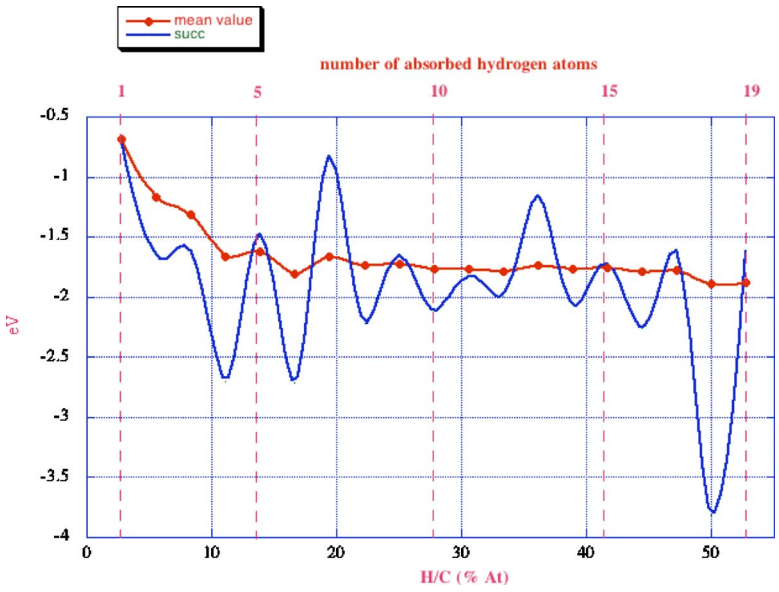

FIG. 2. (Color online) Hydrogen–graphite interaction energy (eV) vs the H/C ratio; "mean value" is calculated using Eq. (2), "succ" using Eq. (1).

the other two atoms. Because of the steric constraints, H#10 cannot absorb contiguously but instead is rejected towards the limit of the crystal cell, on the lower graphene layer.

The other hydrogen atoms are unevenly distributed across the two planes as shown in Fig. 3: out of a total number of 19, only 7 are on the upper plane. This total number corresponds to an H/C ratio of 53% at. All the C-H bonds are more or less parallel to the **c** axis direction. In spite of the steric constraints, the carbon atoms' stacking is maintained much like *ABAB* stacking in pure graphite: half the carbon atoms of a layer are above a carbon of the layer below, and half above the center of a cycle.

The effect of inserting a single hydrogen atom in the total DOS of the system is shown in Fig. 4 (the projection on the hydrogen atom is magnified by a factor of 10). Comparison with Fig. 1 shows a slight perturbation around −9 eV due to the H(1*s*) energy level that combines almost only with the C(π) bands. This observation explains why here the C-H bonds are less energetic than standard chemical C-H bonds in hydrocarbon compounds: H is bonded through a C(π)-H(1*s*) combination, the weight of the C(2*s*) orbitals is negligible while a usual chemical bond is achieved through a C(sp^3)-H(1*s*) or C(sp^2)−H(1*s*) combination where the C(2*s*) orbital weight is similar to the C(2*p*) ones.

The other noticeable information derived from Fig. 4 concerns the region around the Fermi energy level. Since pure graphite is a nonmetal, its electronic zero gap is located between the valence π and conduction π^* bands. The H(1*s*) electron being paired with an originally π electron to form

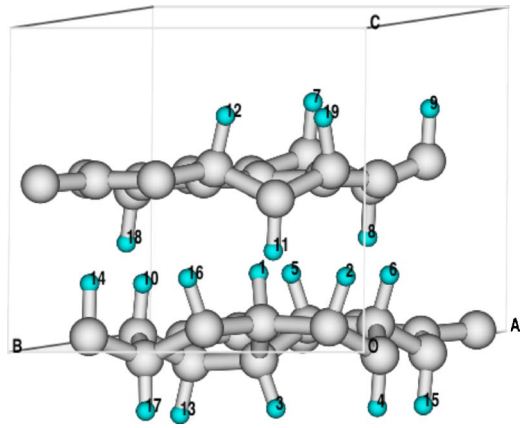

FIG. 3. (Color online) $3\times3\times1$ Crystal working supercell at the end of the hydrogenation process. The number of implanted hydrogen atoms is 19, which corresponds to an H/C ratio of 53%.

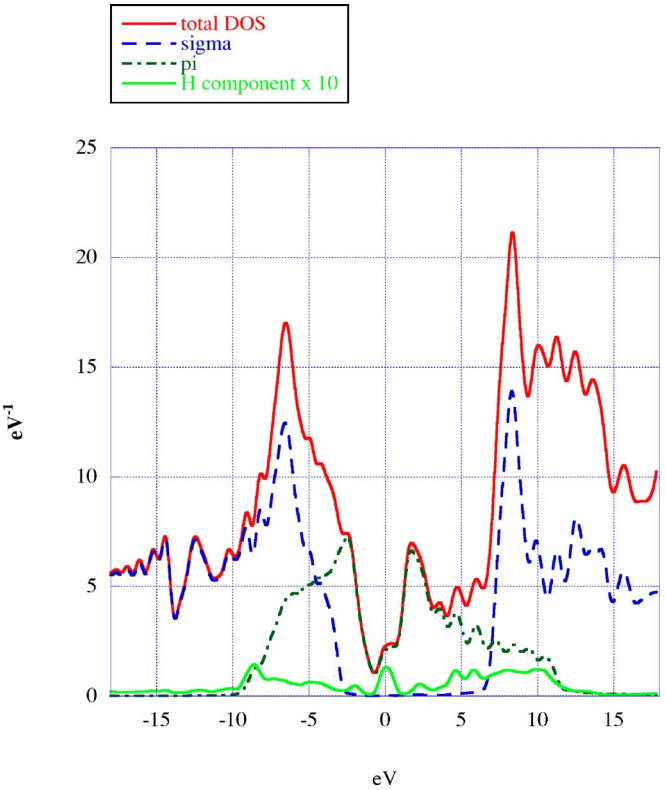

FIG. 4. (Color online) Modification of the graphite DOS after a single hydrogen atom implantation. The projection on the hydrogen atom is magnified by a factor of 10.

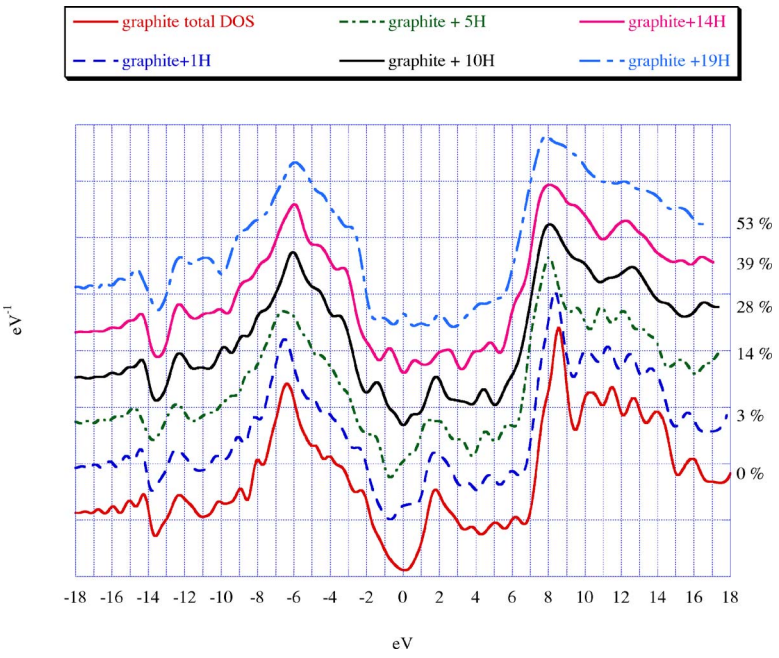

FIG. 5. (Color online) Evolution of the DOS with the hydrogenation ratio from 0 (pure graphite) to saturation. Figure 2 can be referred to in converting the number of absorbed H atoms into the H/C ratio.

the C-H bond, the resulting occupied and virtual CH electronic states are located on each part of the Fermi level, forming the peak visible on the DOS canceling out the gap. This will be the case any time there is an odd number of absorbed hydrogens. H also takes part in this band, if only in the single hydrogen absorption case. In the case of an even number of hydrogen atoms, this band is split into a small feature below the Fermi level and another one above it. Concerning the Fermi level itself, the calculation shows that it increases linearly from 6.9 eV for pure graphite to 8.3 eV for the hydrogen saturated system.

Comparing the total and projected DOSs in the σ valence band (Fig. 4), it must be noted that the area between the two curves was negligible in the case of pure graphite whereas it was noticeable below −10 eV in the hydrogenated structure, although the hydrogen contribution was zero in this area. This indicates that even at low hydrogen content, the electronic density in the interlayer region increases.

The DOS evolution when the H/C ratio is increasing shows that the $C(\pi)-H(1s)$ bonding combination slowly shifts towards the σ C-C band (Fig. 5) until it finally completely merges with it and broadens the σ band. At the end of the process, this band is quite similar to the diamond valence band displayed for comparison in Fig. 6; but its center is 5.9 eV below the Fermi level versus −8.3 eV for diamond, the upper limit being around −2 eV in both cases.

The π band originally situated at −2.3 eV shifts to −1.0 eV. The main π^* peak in the graphite's conduction band tends to decompose progressively. At completion, there remain three very small peaks above the Fermi level corre-

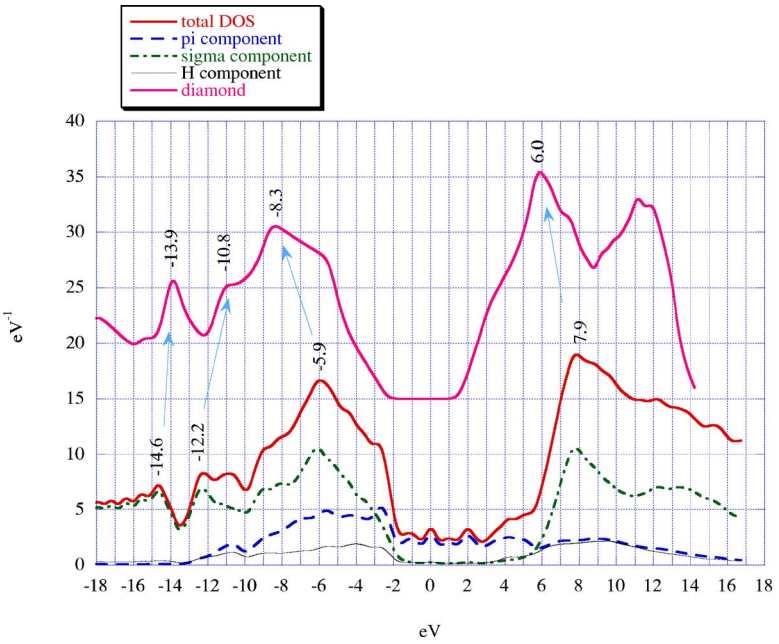

FIG. 6. (Color online) Fully hydrogenated graphite DOS with projection on the σ and π carbon orbitals and on the H(1s). The DOS of diamond is given as a comparison and identification of the main features is pointed to by the arrows.

sponding to the unoccupied energy levels remaining free, and the virtual C(π)-H(1s) energy levels are merged with the σ^* structure. Compared to pure graphite, the structure becomes simpler as the hydrogen rate increases, the four minor peaks in the region 10–18 eV are less and less marked until they almost disappear in the case of the fully hydrogenated system.

Even if only one carbon atom out of two holds a hydrogen atom, most of the carbons are in an $sp^x(x>2)$ hybridization state, except for some atoms on the left part of the upper layer in Fig. 3. As a consequence, the fully hydrogenated structure gives rise to a DOS structure similar in many ways to that of the diamond as can be observed in Fig. 6. The diamond DOS is narrower in the σ conduction band, the C(2s) peak is at −13.9 eV whereas it lies at −14.7 eV for the hydrogenated structure. Also, the diamond's gap between σ and σ^* is occupied by the free π and π^* contributions in the other case. Incidentally, it should be mentioned that, because of the local curvature of the graphene plans, the remaining π orbitals are not necessarily pure C(p_z) orbital but rather a combination of the three p components also with a small s contribution that is not noticeable on the DOSs.[15]

Compared to diamond, the two σ features at −13.9 and −8.3 and the shoulder at −10.8 eV must be likened to the peaks at −14.6, −12.2, and −5.9 eV in the hydrogenated DOS, whereas the peak at −10.8 eV in the same DOS is due to combination with H(1s) projection. In the conduction band also, the diamond σ^* components are shifted to the low energies compared to the fully hydrogenated graphite. Nevertheless, a one-to-one identification of the peaks can be suggested: 6.0, 11.1, and 12.0 eV in the diamond DOS correspond to 7.9, 12.3, and 13.7 eV in the other one (Fig. 6).

An important issue concerning the characterization of more or less graphitic carbons is the evaluation of the ratio ρ=C(sp^3)/C(sp^2). Considering that the carbon atoms in pure perfect graphite are all sp^2, ρ is indicative of the level of amorphization of any carbon sample. Since the hydrogen insertion process implies the transformation of the absorbent carbon hybridization, the present model can be used to propose a tentative criterion.

In the graphite DOS (Fig. 1), the pure π^* band, excluding the interlayer contribution zone extends approximately from 0 to 4 eV. This is also the case for the fully hydrogenated system (Fig. 6). Therefore, the ratio of the DOS area Σ in this zone must be related to ρ. Figure 7 shows the ratio Σ(graphite+nH)/Σ(graphite). The function is not strictly linear because of a certain amount of interlayer contribution and the approximate π orbital definition, but the linear approximation is quite convincing, with a slope of −0.8.

IV. DISCUSSION AND CONCLUSION

The main goal of this work was to propose a quantum model for hydrogen implantation into the first layers below the surface of a graphite sample under nuclear fusion device conditions. This model would also apply to hydrogen insertion into the bulk during diffusion in an ion beam bombarded graphite. The corresponding calculated DOS could then be compared to experimental results.

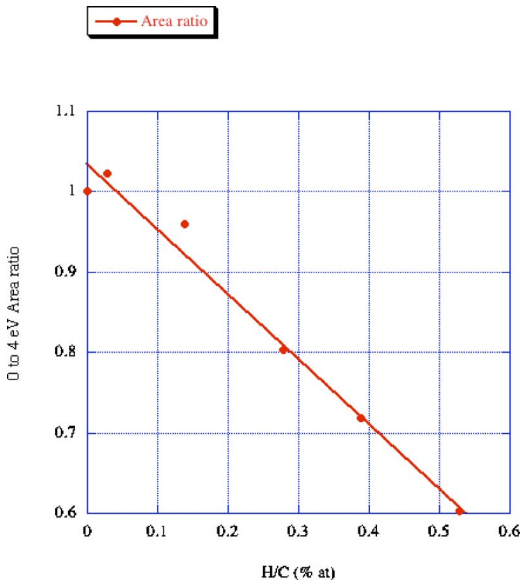

FIG. 7. (Color online) π^* surface area calculated from 0 to 4 eV on the spectra displayed in Fig. 5, relative to pure graphite and as a function of the implantation ratio.

The working crystal cell chosen for this purpose is of course small in regard of the samples used during the spectroscopic experiments but it nevertheless provides reliable information.

For example, the larger number of atomic hydrogens this cell can incorporate is 19, which represents an H/C ratio of 53%. This ratio is not very different from experimental results. It also a posteriori and empirically validates our method which keeps the graphite lattice parameters unchanged.

Under tokamak discharge conditions, it has been determined that at room temperature the upper limit of the implanted hydrogen content was 45% at. in the near surface region.[13,31] Another source indicates about 40% H/C (Ref. 32) in laboratory simulation by hydrogen ions bombardment at room temperature.

Nevertheless, the H/C 40% ratio corresponds to implantation of 14 Hs in the working cell and it can be seen that the two upper spectra in Fig. 5 (H/C 53 and 40 %) are not qualitatively different, but the π peak in the saturated system is split into −1.0 and 0.6 eV in the 14 H system. Therefore, the discussion can revolve around the fully hydrogenated system.

Ugolini *et al.*[13] have studied the effect of bombardment of HOPG and polycrystalline graphite by energetic hydrogen ions using UPS (He I and He II) techniques. On both systems they observed a fairly structureless valence band at about 7.5 eV and a shoulder near 4 eV. This corresponds fairly well with the broad σ band in Fig. 6 whose maximum is at −5.9 eV (the inversion of sign − to + is due to experimental conventions) and the shoulder at −2.8 eV corresponding to a distance between the two features of 3.2 eV versus 3.5 eV in UPS (He II).

In the same study, the EELS spectrum for the original graphite shows an energy loss of 6.6 eV from the $\pi-\pi^*$ transition. This signal strongly decreases in intensity, be-

comes broader and shifts to a lower energy loss of 4.6 eV after bombardment. It is difficult to make an exact comparison but the quantum DOS shows the same tendency. The quantum $\pi-\pi^*$ transition energy between the two main peaks is nevertheless smaller, 3 eV. This could be due to the potential the C($1s$) electron system exerts on the valence electrons: the calculations are performed using a standard pseudo-potential generated by a complete $1s^2$ C electron core whereas the EELS techniques creates a hole in this shell.

The same problem arises during comparison with X-ray electron spectroscopy. This kind of technique is often used to investigate the π electronic structure of hydrogenated carbons (graphite or amorphous) at different hydrogen contents. More generally, the evolution of the π-type signals is indicative of the level of disorder in a poorly organized carbonaceous material, whether hydrogenated or not. For example, Lascovich *et al.*[14] compared the Auger experimental DOS with the ab initio MD of *a*-C. Both techniques show a broadening of the structures in the binding region from E_F to −10 eV. This is also the case in our Figs. 5 and 6. Moreover, the Auger C KVV spectrum shows a strong peak at 1.2 eV. The MD derived DOS shows only a shoulder at this energy level but our Fig. 5 indicates that at H/C=28% there appears a strong peak at −1.4 eV growing towards −0.7 eV for H/C=40%. The same paper indicated that the sample density is 2.2 g/cm^3 and that the numerical simulations assign this density an sp^3 ratio of 19% whereas this ratio would be of 38% for a density not much different from 2.4 g/cm^3; therefore the agreement with the quantum results is more than purely qualitative taking into account that the sp^2 content is not measured but only indirectly estimated. The Auger spectra also show strong structures at −4.3 and −5.5 eV, they correspond to the strong shoulders at −3.5 and −4.5 eV in Fig. 5, growing with the hydrogenation ratio.

In the same domain of *X*-absorption spectroscopy, Díaz *et al.*, in their NEXAFS study,[19] used the area of the π^* resonance as a measure of the total density of the π^* unoccupied states of *a*-C films, which is equivalent to our Fig. 7. They reported that π^* states with non-negligible density extend up to 10 eV in pure graphite, as opposed to only up to 5 eV in highly sp^3 bonded *a*-C films. The present value for the fully hydrogenated system is very close: 5.6 eV.

As a conclusion, without claiming that amorphous carbon can be likened to hydrogenated graphite, the present study contributes to emphasizing their similarities at least concerning the sp^3/sp^2 relative proportions. Therefore, bulk hydrogenated graphite can be proposed as a model and a tool in quantifying this ratio in carbonaceous materials. This is also a consequence of the similitude between the CH and CC chemical bonds with respect to their electronic structure. Because of this similitude, the electronic density of states continuously evolves from the DOS of pure graphite to a DOS rather similar to that of diamond's as the H/C ratio grows from zero to its upper limit, which should be 1, as clearly substantiated by Figs. 5 and 6.

ACKNOWLEDGMENTS

This work is supported by the Euratom-CEA Association in the framework of the LRC (Laboratoire de Recherche Conventionné CEA/DSM – Université de Provence PIIM). All the calculations were performed at IDRIS, the CNRS computing center.

*Corresponding author. Email address: alain.allouche@up.univ-mrs.fr

[1] H. Atsumi, J. Nucl. Mater. **313**, 543 (2003).
[2] M. Mayer, V. Philipps, P. Wienhold, H. G. Esser, J. von Seggern, and M. J. Rubel, J. Nucl. Mater. **290**, 381 (2001).
[3] D. D. R. Summers, M. N. A. Beurskens, J. P. Coad, G. Counsell, W. Fundamenski, G. F. Matthews, and M. F. Stamp, J. Nucl. Mater. **290**, 496 (2001).
[4] G. Federici, R. A. Anderl, P. Andrew, J. N. Brooks, R. A. Causey, J. P. Coad, D. Cowgill, R. P. Doerner, A. A. Haasz, G. Janeschitz, W. Jacob, G. R. Longhurst, R. Nygren, A. Peacock, M. A. Pick, V. Philipps, J. Roth, C. H. Skinner, and W. R. Wampler, J. Nucl. Mater. **266**, 14 (1999).
[5] A. A. Haasz, P. Franzen, J. W. Davis, S. Chiu, and C. S. Pitcher, J. Appl. Phys. **77**, 66 (1995).
[6] M. A. De La Casa-Lillo, F. Lamari-Darkrim, D. Cazorla-Amoros, and A. Linares-Solano, J. Phys. Chem. B **106**, 10930 (2002).
[7] J. Li and S. Yip, J. Chem. Phys. **119**, 2376 (2003).
[8] M. Rzepka, E. Bauer, G. Reichenauer, T. Schliermann, B. Bernhardt, K. Bohmhammel, E. Henneberg, U. Knoll, H.-E. Maneck, and W. Braue, J. Phys. Chem. B **109**, 14979 (2005).
[9] A. Allouche, A. Jelea, F. Marinelli, and Y. Ferro, Phys. Scr., T **T124**, 91 (2006).
[10] Y. Ferro, A. Jelea, F. Marinelli, C. Brosset, and A. Allouche, J. Nucl. Mater. **337**, 897 (2005).
[11] A. Allouche and Y. Ferro, Carbon. **44**, 3320 (2006).
[12] A. Allouche, Y. Ferro, T. Angot, C. Thomas, and J.-M. Layet, J. Chem. Phys. **123**, 124701 (2005).
[13] D. Ugolini, J. Eitle, and P. Oelhafen, Appl. Phys. A: Solids Surf. **54**, 57 (1992).
[14] J. C. Lascovich, V. Rosato, and A. Santoni, Surf. Sci. **467**, 139 (2000).
[15] L. Calliari, Diamond Relat. Mater. **14**, 1232 (2005).
[16] J. T. Titantah and D. Lamoen, Phys. Rev. B **70**, 075115 (2004).
[17] P. K. Chu and L. Li, Chem. Phys. **96**, 253 (2006).
[18] N. Bernier, F. Bocquet, A. Allouche, W. Saïkaly, C. Brosset, J. Thibault, and A. Charaï (to be published).
[19] J. Díaz, S. Anders, X. Zhou, E. J. Moler, S. A. Kellar, and Z. Hussain, Phys. Rev. B **64**, 125204 (2005).
[20] R. Gago, M. Vinnichenko, H. U. Jäger, A. Y. Belov, I. Jiménez, N. Huang, H. Sun, and M. F. Maitz, Phys. Rev. B **72**, 014120 (2005).
[21] J. P. Perdew, K. Burke, and M. Ernzerhof, Phys. Rev. Lett. **77**, 3865 (1996).
[22] K. Laasonen, A. Pasquarello, R. Car, C. Lee, and D. Vanderbilt, Phys. Rev. B **47**, 10142 (1993).

[23] H. J. Monkhorst and J. D. Pack, Phys. Rev. B **13**, 5188 (1972).
[24] S. Baroni, A. Dal Corso, S. de Gironcoli, P. Giannozzi, C. Cavazzoni, G. Ballabio, S. Scandolo, G. Chiarotti, P. Focher, A. Pasquarello, K. Laasonen, A. Trave, R. Car, N. Marzari, and A. Kokalj, http://www.pwscf.org/.
[25] J. C. Charlier, X. Gonze, and J. P. Michenaud, Phys. Rev. B **43**, 4579 (1991).
[26] D. A. Fisher, R. M. Wentzcovitch, R. G. Carr, A. Continenza, and A. J. Freeman, Phys. Rev. B **44**, 1427 (1991).
[27] L. Jeloaica and V. Sidis, Chem. Phys. Lett. **300**, 157 (1999).
[28] X. Sha and B. Jackson, Surf. Sci. **496**, 318 (2002).
[29] Y. Ferro, F. Marinelli, and A. Allouche, J. Chem. Phys. **116**, 8124 (2002).
[30] Y. Ferro, F. Marinelli, and A. Allouche, Chem. Phys. Lett. **368**, 609 (2003).
[31] Y. Gotoh, J. Nucl. Mater. **248**, 46 (1997).
[32] R. F. Willis, B. Fitton, and G. S. Painter, Phys. Rev. B **9**, 1926 (1974).